

**SIMULATION, CHARACTERIZATION AND
ANALYSIS OF SILICON GERMANIUM AND POLY
(TRIARYLAMINE) HETEROJUNCTION FOR
PROSPECTIVE PHOTO-DEVICES**

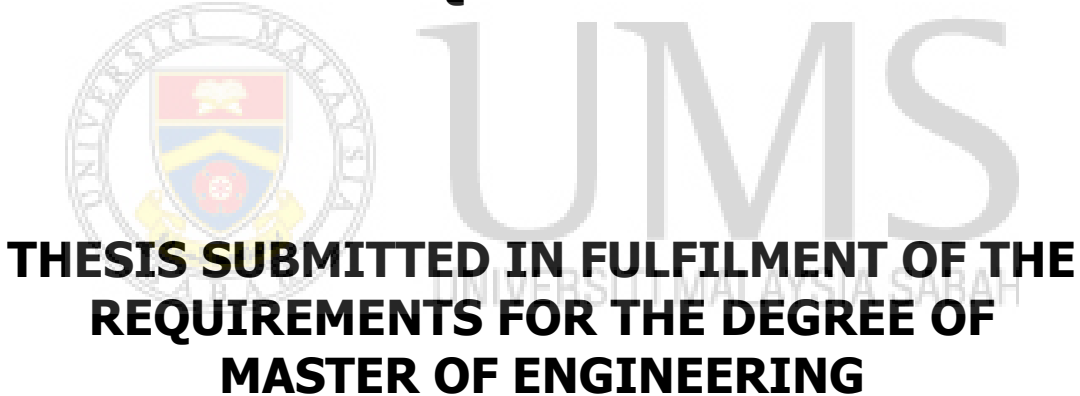


UMS
UNIVERSITI MALAYSIA SABAH

**FACULTY OF ENGINEERING
UNIVERSITI MALAYSIA SABAH
2023**

**SIMULATION, CHARACTERIZATION AND
ANALYSIS OF SILICON GERMANIUM AND POLY
(TRIARYLAMINE) HETEROJUNCTION FOR
PROSPECTIVE PHOTO-DEVICES**

NUR SYAFIQA BINTI MD NASIR



**THESIS SUBMITTED IN FULFILMENT OF THE
REQUIREMENTS FOR THE DEGREE OF
MASTER OF ENGINEERING**

**FACULTY OF ENGINEERING
UNIVERSITI MALAYSIA SABAH
2023**

UNIVERSITI MALAYSIA SABAH
BORANG PENGESAHAN STATUS TESIS

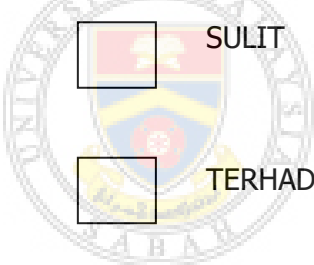
JUDUL : **SIMULATION, CHARACTERIZATION AND ANALYSIS OF SILICON GERMANIUM AND POLY (TRIARYLAMINE) HETEROJUNCTION FOR PROSPECTIVE PHOTO-DEVICES**

IJAZAH : **SARJANA KEJURUTERAAN**

BIDANG : **KEJURUTERAAN ELEKTRIK DAN ELEKTRONIK**

Saya **NUR SYAFIQA BINTI MD NASIR**, Sesi **2020-2023**, mengaku membenarkan tesis Sarjana ini disimpan di Perpustakaan Universiti Malaysia Sabah dengan syarat-syarat kegunaan seperti berikut:-

1. Tesis ini adalah hak milik Universiti Malaysia Sabah
2. Perpustakaan Universiti Malaysia Sabah dibenarkan membuat salinan untuk tujuan pengajian sahaja.
3. Perpustakaan dibenarkan membuat salinan tesis ini sebagai bahan pertukaran antara institusi pengajian tinggi.
4. Sila tandakan (/):



SULIT

TERHAD

/

TIDAK TERHAD

(Mengandungi maklumat yang berdarjah keselamatan atau kepentingan Malaysia seperti yang termaktub di dalam AKTA RAHSIA 1972)

(Mengandungi maklumat TERHAD yang telah ditentukan oleh organisasi/badan di mana penyelidikan dijalankan)

NUR SYAFIQA BINTI MD NASIR
MK2011010T

Disahkan Oleh,
ANITA BINTI ARSAD
PUSTAKAWAN KANAN
UNIVERSITI MALAYSIA SABAH
(Tandatangan Pustakawan)

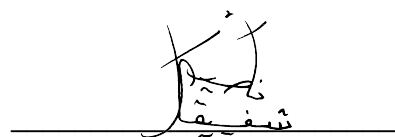
Tarikh : 13 Oktober 2023

(Dr. Bablu Kumar Ghosh)
Penyelia Utama

DECLARATION

I hereby declare that the material in this thesis is my own except for equations, summaries, and references, which have been duly acknowledged.

13 July 2023



Nur Syafiqah binti Md Nasir

MK2011010T



UMS
UNIVERSITI MALAYSIA SABAH

CERTIFICATION

NAME : **NUR SYAFIQA BINTI MD NASIR**
MATRIC NO. : **MK2011010T**
TITLE : **SIMULATION, CHARACTERIZATION AND ANALYSIS OF SILICON GERMANIUM AND POLY (TRIARYLAMINE) HETEROJUNCTION FOR PROSPECTIVE PHOTO-DEVICES**
DEGREE : **MASTER OF ENGINEERING**
FIELD : **ELECTRICAL AND ELECTRONICS**
VIVA DATE : **13 JULY 2023**

CERTIFIED BY

1. **MAIN SUPERVISOR**
DR. BABLU KUMAR GHOSH
2. **CO-SUPERVISOR**
ASSOC. PROF. DR. CHEE FUEI PIEN

Signature



ACKNOWLEDGEMENT

First, praise to Allah for His wonderful route that He has made for me and giving me incredible strength to complete this dissertation.

I would like to extend my gratitude to my supervisor, Dr. Bablu Kumar Ghosh for his guidance, highest patience on my writing skills, constructive comments on my article and continuous encouragement throughout this study. I also would like to thank my co-supervisor Assoc. Prof. Dr. Chee Fuei Pien for her ideas, support and highest patience.

Furthermore, not to forget my lovely parents (Abi and Umi), my siblings (Ila, Ame, Wawa and Adik), my loved one, my great and supportive roommates (Vonnie, Qila and Feli). They have always been by my side dealing with sensitive and emotional part of me. I would not make this far without them.

I would also like to thank my lab mates: Kak Flo for being my partner in crime and healing partner, Auni, my partner in crime, Kak Ros is the one who always teach me how to use spin coater and AFM, Miv is the one who teach me how to deal with sputtering machine as well as AFM machine, Izzuddin is the one who gives out any information about lab, Fenny is the one who drives us anywhere, anytime and Sakinah, my dearest junior. These journey indeed the toughest one.

Not to forget, my utmost gratitude to Universiti Malaysia Sabah, especially Centre for Postgraduate Studies, Centre of Research and Innovation and Material Science Laboratory FSSA for providing facilities and research grants needed to further my studies. May Allah smoothen everyone's path and rezq in their life.

NUR SYAFIQA BINTI MD NASIR

13 July 2023

ABSTRACT

Silicon (Si) is a common electrical and optoelectronic materials technology in the semiconductor industry. Furthermore, transparent device applications with visible to near-infrared band absorption edge shifting are sought. Germanium (Ge) is a promising material that enhances absorption and greater carrier mobility of electronic devices. Poly (triarylamine) (PTAA) in room temperature deposition scope, and as an excellent p-type conductive polymer, it has good visible band transparency. This study initially investigated the PTAA/SiGe and PTAA/Si prospective photo device performance using Solar Cell Capacitance Simulator (SCAPS) software simulation. PTAA thin films are developed using the spin coating process, and SiGe thin films are deposited by the radio frequency sputtering method. The active SiGe morphology is varied by varying the % of Ge composition in SiGe materials and deposition time. In contrast, PTAA morphology is set with a fixed number of drops and spin coating device rotational speed. The structural, compositional, and surface characterisations are performed by x-ray diffraction, scanning electron microscopy with energy dispersive x-ray spectroscopy, and atomic force microscopy, respectively. The ultraviolet-visible spectroscopy for optical and source measurement unit (SMU-2400) instruments for current density - voltage characterizations are also investigated in this study. The SCAPS simulation of $0.3\text{ }\mu\text{m}$ SiGe revealed very high current density (48.1 mA/cm^2) and the highest 8.55% photo-electrical energy conversion efficiency in contrast to similar thickness Si photovoltaic technology is revealed. $\text{Si}_{0.8}\text{Ge}_{0.2}$ has the highest 36.78 nm grain size and $52.49\text{ }\mu\text{m}^{-2}$ grain density and at $800\text{ }^\circ\text{C}$ annealing temperature is achieved. Transparency analysis has shown that the $\text{Si}_{0.8}\text{Ge}_{0.2}$ deposited after 30 minutes is highly transparent for visible light in the wavelength range of 600-700 nm. The highest transparency of $\text{Si}_{0.8}\text{Ge}_{0.2}$ at $600\text{ }^\circ\text{C}$ is realized at 87.87%. $\text{Si}_{0.8}\text{Ge}_{0.2}$ deposited is shown 5.19 rectifying ratio, while $\text{Si}_{0.9}\text{Ge}_{0.1}$ is 7.67. However, both $\text{Si}_{0.8}\text{Ge}_{0.2}$ and $\text{Si}_{0.9}\text{Ge}_{0.1}$ deposited on quartz substrate is revealed at 14.76 and 7.91 rectifying ratio respectively. From simulation result, PTAA/SiGe microstructure is shown preferable than PTAA/Si microstructure and experimental work $\text{Si}_{0.8}\text{Ge}_{0.2}$ is revealed more promising than $\text{Si}_{0.9}\text{Ge}_{0.1}$.

ABSTRAK

SIMULASI, PENCIRIAN, DAN ANALISIS SILIKON GERMANIUM DAN POLI (TRIARILAMIN) HETERO-SIMPANG UNTUK PERANTI FOTO PROSPEKTIF

Silikon (Si) ialah teknologi bahan elektrik dan optoelektronik dalam industri semikonduktor. Tambahan pula, pencarian peralihan sudut penyerapan jalur inframerah boleh dilihat menggunakan aplikasi peranti lutsinar. Germanium (Ge) dapat meningkatkan penyerapan dan mobiliti pembawa dalam sesebuah peranti elektronik. Poli (triarilamin) (PTAA) bersuhu rendah, dapat menghasilkan polimer yang baik, serta mempunyai kadar ketelusan cahaya yang tinggi, di mana bahan tersebut mempunyai kadar ketelusan yang baik. Kajian ini menyiasat tentang prestasi PTAA/SiGe dan PTAA/Si menggunakan simulasi perisian SCAPS. PTAA menggunakan proses salutan putaran dan SiGe menggunakan kaedah percikan frekuensi radio. Berbeza dengan morfologi, PTAA diset dengan bilangan titisan yang ditetapkan dan kelajuan salutan putaran. Pencirian struktur, optik, dan elektrik menggunakan pembelauan sinar-x, pengimbasan mikroskopi elektron dengan spektroskopi sinar-x penyebaran tenaga, dan mikroskop daya atom. Spektroskopi ternampakkan ultraviolet digunakan untuk pencirian optik manakala instrument unit ukuran sumber (SMU-2400) untuk ketumpatan arus-voltan telah dikaji dalam kajian ini. Simulasi SCAPS pada $0.3 \mu\text{m}$ SiGe menunjukkan ketumpatan arus tinggi (48.1 mA/cm^2) dan kecekapan peranti pada 8.55% menunjukkan nilai tinggi berbanding teknologi Si pada ketebalan sama. Struktur $\text{Si}_{0.8}\text{Ge}_{0.2}$ dicapai pada saiz butiran yang besar dan juga ketumpatan butiran tinggi, masing-masing 36.78 nm dan $52.49 \mu\text{m}^2$ pada 800°C . Analisis ketelusan cahaya menunjukkan $\text{Si}_{0.8}\text{Ge}_{0.2}$ yang dipercikkan selepas 30 minit sangat telus cahaya pada julat gelombang $600\text{-}700 \text{ nm}$. Nilai ketelusan cahaya bagi $\text{Si}_{0.8}\text{Ge}_{0.2}$ pada 600°C adalah 87.87%. $\text{Si}_{0.8}\text{Ge}_{0.2}$ yang dimendapkan mempunyai jumlah nisbah kelurusan tinggi iaitu 5.19, manakala $\text{Si}_{0.9}\text{Ge}_{0.1}$ telah dimendapkan hanya 7.67. Namun begitu, kedua-dua $\text{Si}_{0.8}\text{Ge}_{0.2}$ and $\text{Si}_{0.9}\text{Ge}_{0.1}$ yang dimendapkan pada substrat kuarza yang mempunyai nisbah kelurusan yang tinggi, masing-masing pada 14.76 dan 7.91. Simulasi mikro-struktur PTAA/SiGe diutamakan daripada mikro-struktur PTAA/Si dan kerja uji kaji $\text{Si}_{0.8}\text{Ge}_{0.2}$ adalah lebih baik berbanding $\text{Si}_{0.9}\text{Ge}_{0.1}$.

LIST OF CONTENTS

	Page
TITLE	i
DECLARATION	ii
CERTIFICATION	iii
ACKNOWLEDGEMENT	iv
ABSTRACT	v
ABSTRAK	vi
LIST OF CONTENTS	xi
LIST OF TABLES	xiv
LIST OF FIGURES	xvi
LIST OF SYMBOLS	xx
LIST OF ABBREVIATONS	xxii
LIST OF APPENDIX	xxv
CHAPTER 1: INTRODUCTION	
1.1 Research Background	1
1.2 Problem Statement	3
1.3 Research Objectives	4
1.4 Research Contribution	4
1.5 Thesis Structure	5
CHAPTER 2: LITERATURE REVIEW	
2.1 Overview	7
2.2 Photo Device	8
2.3 Classification of Semiconductor	11
2.3.1 Inorganic Semiconductor	11
2.3.2 Organic Semiconductor	15
2.4 SCAPS Simulation for Hybrid Cell	18

2.5	Hybrid Photo Device	20
2.5.1	Hybrid Semiconductor Structure for Photo Device Cell	21
2.5.2	Electrical Properties of Hybrid Device	22
2.6	Research Direction	26

CHAPTER 3: RESEARCH METHODOLOGY

3.1	Overview	27
3.2	Research Methodology Flow Chart	27
3.3	Classification of Materials	29
3.3.1	Type of Substrates	29
3.4	Material Parameter for SCAPS Simulation	32
3.4.1	Parameter for PTAA and SiGe Material	32
3.4.2	Parameter for n-type Si and SiGe Material with and without Passivation Layer SiO_2	34
3.4.3	Parameter for PEDOT: PSS and PTAA Material as an Absorber Layer	36
3.5	Material	39
3.5.1	Type of Substrates	39
3.5.2	Technique for Thin Film Depositions	40
3.5.3	Hybrid Inorganic-Organic Photo Device Cell	45
3.6	Thin Film and Hybrid Photo Device Cell Characterization Method	49
3.6.1	Structural Properties of Thin Films	49
3.6.2	Surface Morphology	52
3.6.3	Optical Morphology	53
3.7	Current Density-Voltage (J-V) Characterization Analysis	55

CHAPTER 4: RESULT AND DISCUSSION ON SIMULATION WORK

4.1	Overview	57
4.2	J-V Electrical Characterization	57
4.2.1	Current Density-Voltage (J-V) Analysis	57

4.2.2	External Quantum Efficiency (EQE) Analysis	68
CHAPTER 5: RESULT AND DISCUSSION FOR PTAA/SiGe HYBRID DEVICE		
5.1	Overview	72
5.2	Parameter for Thin Films	72
5.2.1	PTAA Thin Film Characterization	73
5.2.2	SiGe Thin Film Characterization Effect on Different Annealing Temperatures	78
5.2.3	SiGe Thin Film Composition Effect on Different Thickness Depositions	89
5.3	Direct current (DC) Electrical Characterization	100
5.3.1	Current Density-Voltage (J-V) Analysis	100
CHAPTER 6: CONCLUSION AND RECOMMENDATION		
6.1	Overview	111
6.2	Summary	111
6.3	Future Recommendation	113
REFERENCES		
APPENDIX		

LIST OF TABLES

		Page
Table 2.1	: Past Research on Numerical Analysis Using SCAPS-1D	19
Table 2.2	: List of Past Research on Hybrid Si and SiGe Cells	24
Table 3.1	: The Parameter for The Hybrid Photo Device	34
Table 3.2	: The Parameter for PTAA, SiO_2 , Si and SiGe of SCAPS Simulation	35
Table 3.3	: The Parameter for pPTAA, pPEDOT: PSS, SiO_2 , and nSiGe in SCAPS Simulation	37
Table 4.1	: The Electrical Conductivity of Hybrid Device Based on J-V Graph Simulation	59
Table 5.1	: The Grain Size and Surface Roughness Analysis for Varied Deposition Layer Of PTAA	75
Table 5.2	: The Transmittance at Specific Wavelength for Visible Light and Near Infrared	78
Table 5.3	: The Structural Properties for XRD Data	80
Table 5.4	: The Summary for Structural Properties for Both SiGe Composition Using AFM Analysis	84
Table 5.5	: The Summary of Transmittance at 850 nm Wavelength and Bandgap for Both SiGe Composition from Absorption Graph	85
Table 5.6	: The Structural Morphology from XRD Data	91
Table 5.7	: The AFM Analysis for Surface Roughness of Different Compositions of $\text{Si}_{0.8}\text{Ge}_{0.2}$ and $\text{Si}_{0.9}\text{Ge}_{0.1}$	95
Table 5.8	: The AFM Analysis for Grain Size of Different Compositions of $\text{Si}_{0.8}\text{Ge}_{0.2}$ and $\text{Si}_{0.9}\text{Ge}_{0.1}$	96
Table 5.9	: The Transmittance for Both Compositions of SiGe Thin Film at Different Wavelengths of Visible Light and NIR with Different Deposition Times and Substrates	97
Table 5.10	: The Optical Bandgap for Both SiGe Compositions Deposited onto ITO and Quartz Glass Substrate	99
Table 5.11	: The Rectifying Ratio for Both SiGe Composition Deposited	103

	onto ITO Glass Substrate at Different Deposition Times	
Table 5.12	: The Rectifying Ratio for Both SiGe Composition Deposited onto Quartz Glass Substrate at Different Deposition Times	106
Table 5.13	: The Ideality Factor for Both $\text{Si}_{0.8}\text{Ge}_{0.2}$ and $\text{Si}_{0.9}\text{Ge}_{0.1}$ Deposited on ITO And Quartz Glass Substrates	107
Table 5.14	: The Rectifying Ratio for Dark and Light Illumination for Both SiGe Photo Devices	110



LIST OF FIGURES

	Page
Figure 2.1 : Graphical Mechanism of Photo Device Cell	11
Figure 2.2 : Types of Inorganic Material used in Photo Device Cell	13
Figure 2.3 : Several Example of Organic Material for Photo Diode and Photovoltaic	16
Figure 2.4 : The Chemical Structure for PTAA Organic Material	17
Figure 2.5 : The Action Panel in the SCAPS Programme Cell Simulator	18
Figure 3.1 : Flow Chart of Research Methodology	28
Figure 3.2 : The SCAPS Software (a) Simulation Window and (b) the Design Layout for the Simulation	31
Figure 3.3 : The Parameter for (a) PTAA and (b) SiGe Thin Film in SCAPS Simulator	33
Figure 3.4 : The (a) Arrangement and (b) SCAPS Model for Emerging Cell	35
Figure 3.5 : The Schematic Diagram for Both (a) without SiO_2 Passivated Layer and (b) With SiO_2 Passivated Layer for nSiGe Absorber Layer	39
Figure 3.6 : (a) ITO Glass and (b) Quartz Glass Substrates	40
Figure 3.7 : RF Sputtering Schematic for Deposit an Inorganic Material Thin Film	42
Figure 3.8 : RF Sputtering Method for the Deposition of Inorganic Material Thin Film	43
Figure 3.9 : Spin Coating Method for the Deposition of Organic Thin Film onto the Substrate	44
Figure 3.10 : The Annealing Process for Thin Film	45
Figure 3.11 : Design for Hybrid Inorganic-Organic Photo Device Deposited onto (a) ITO and (b) Quartz Glass	46
Figure 3.12 : Graphical Methodology for RF Sputtering Process	47
Figure 3.13 : Graphical Method for Preparing PTAA Solution and Depositing PTAA Thin Film	48

Figure 3.14	: Step by Step Process for the Fabrication of Hybrid Inorganic-Organic Photo Device: (a) Cleaned ITO and Quartz Substrate, (b) ITO and Ag Quartz Masked with Kapton Tape, (c) n-SiGe Thin Film Deposited onto the Substrate, (d) p-PTAA Spin-Coated onto the SiGe Layer, (e) Silver Paste Layered onto the p-PTAA Thin Film and (f) Hybrid Inorganic-Organic Photo Device	48
Figure 3.15	: Geometrical Condition for Diffraction of Lattice Plane	50
Figure 3.16	: SEM Schematic to Analyse the Structural Morphology of Sample	52
Figure 3.17	: The Schematic Diagram for AFM Machine	53
Figure 3.18	: The Mechanism of UV-Vis Spectroscopy	54
Figure 3.19	: The Layout of Keithley 2400 2-Probes Source Meter for J-V Characterization	56
Figure 4.1	: Current Density-Voltage Graph for Different Thicknesses of Emitter Layer	58
Figure 4.2	: The Graph of (a) Open-Circuit, Voc, (b) Short-Circuit Current, Jsc, (c) Fill Factor, FF, and (d) Efficiency for Different SiGe Layer Thicknesses	60
Figure 4.3	: The (a) Open-Circuit Voltage, (b) Short-Circuit Current, (c) Fill Factor, and (d) Efficiency for various Thicknesses of nSi and nSiGe Active Layer without SiO ₂ Passivated Layer	61
Figure 4.4	: (a) Voc; (b) Jsc, (c) FF, and (d) Efficiency for Diverse Passivated SiO ₂ Layer Thickness to be Inserted into the Active Layer	63
Figure 4.5	: (a) Jsc and (b) Efficiency for Thin Active Layer Thickness of nSi and nSiGe at 300 K And 330 K Operating Temperature for 2 nm SiO ₂ Layer Thickness	64
Figure 4.6	: (a) Efficiency, (b) Voc, (c) Jsc, and (d) FF Result for Both PEDOT: PSS and PTAA with nSiGe Active Layer without SiO ₂ Passivated Layer	65

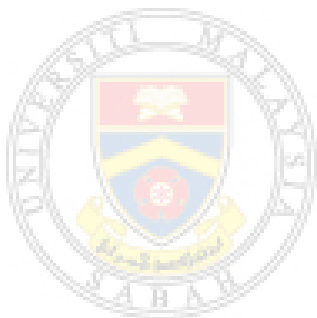
Figure 4.7	: (a) Efficiency, (b) Voc, (c) J _{sc} , and (d) FF Result for Both PEDOT: PSS and PTAA with nSiGe Active Layer Include SiO ₂ Passivated Layer	66
Figure 4.8	: Defect Density Graph that Correlated to Efficiency for (a) PEDOT: PSS/SiO ₂ /nSiGe and (b) PTAA/SiO ₂ /nSiGe	67
Figure 4.9	: The External Quantum Efficiency for Different Thicknesses of Emitter Layer	69
Figure 4.10	: Quantum Efficiency Variation of p-PTAA/SiO ₂ /nSiGe; p-PTAA/SiO ₂ /nSi and p-PTAA/nSiGe; p-PTAA/nSi devices	70
Figure 5.1	: The XRD Data for (a) 1 Layer, (b) 3 Layers, and (c) 5 Layer of PTAA Thin Film at 1000 rpm	73
Figure 5.2	: The Thickness for (a) 1 Layer, (b) 3 Layers, and (c) 5 Layers of PTAA Thin Film	74
Figure 5.3	: The Graph of (a) Transmittance and (b) Absorption for Different Deposition of PTAA Thin Film	77
Figure 5.4	: XRD Result for (a) Si _{0.8} Ge _{0.2} and (b) Si _{0.9} Ge _{0.1} Composition	79
Figure 5.5	: AFM Analysis for Both Crystalline Si _{0.8} Ge _{0.2} at (a) 600 °C (b) 700 °C, and (c) 800 °C and Si _{0.9} Ge _{0.1} (d) 600 °C (e) 700 °C, and (f) 800 °C	82
Figure 5.6	: The Crystallite Size and RMS Roughness Graph Against Annealing Temperature for Both (a) Si _{0.8} Ge _{0.2} and (b) Si _{0.9} Ge _{0.1}	83
Figure 5.7	: Transmittance Graph for (a) Si _{0.8} Ge _{0.2} and (b) Si _{0.9} Ge _{0.1} at 600 °C, 700 °C, and 800 °C.	87
Figure 5.8	: The Energy Vs $(ahv)^2$, Band Gap Graph for (a) Si _{0.8} Ge _{0.2} and (b) Si _{0.9} Ge _{0.1} Composition	87
Figure 5.9	: Absorbance Shift for (a) Si _{0.8} Ge _{0.2} and (b) Si _{0.9} Ge _{0.1} Thin Film at Different Annealing Temperatures	88
Figure 5.10	: XRD Data for Different Time Deposition on Quartz Substrate for (a) Si _{0.8} Ge _{0.2} and (b) Si _{0.9} Ge _{0.1}	90
Figure 5.11	: The EDX Graph and Atom Concentration for SiGe Deposited on Quartz Glass at 800 °C Annealing Temperature for 30	92

	Minutes Deposition Time	
Figure 5.12	: The AFM Analysis for $\text{Si}_{0.8}\text{Ge}_{0.2}$ at Deposition Time (a) 30 Minutes, (b) 60 Minutes, (c) 90 Minutes and $\text{Si}_{0.9}\text{Ge}_{0.1}$ with Deposition Time (d) 30 Minutes, (e) 60 Minutes, and (f) 90 Minutes Deposited onto ITO Glass Substrate	92
Figure 5.13	: The AFM Thickness Image for $\text{Si}_{0.8}\text{Ge}_{0.2}$ at (a) 30 Minutes, (b) 60 Minutes, (c) 90 Minutes Time Deposition and Composition $\text{Si}_{0.9}\text{Ge}_{0.1}$ at (d) 30 Minutes, (e) 60 Minutes, and (f) 90 Minutes Time Deposition Deposited onto Quartz Glass Substrate	94
Figure 5.14	: The Graph of Transmittance for Both Composition $\text{Si}_{0.8}\text{Ge}_{0.2}$ And $\text{Si}_{0.9}\text{Ge}_{0.1}$ Deposited Onto (a) ITO and (b) Quartz Glass Substrate	97
Figure 5.15	: The Absorption Graph for Both SiGe Compositions Deposited onto (a) ITO and (b) Quartz Glass Substrate	98
Figure 5.16	: The Optical Bandgap for Both Composition of SiGe Deposited on (a) ITO and (b) Quartz Glass Substrate	99
Figure 5.17	: The J-V Graph for $\text{Si}_{0.8}\text{Ge}_{0.2}$ Composition For (a) White Light and (b) Infrared Condition	101
Figure 5.18	: The Semilog J-V Graph for $\text{Si}_{0.9}\text{Ge}_{0.1}$ Effect on (a) White Light and (b) Infrared Condition	102
Figure 5.19	: The J-V Graph for $\text{Si}_{0.8}\text{Ge}_{0.2}$ Effect on (a) White Light and (b) Red Light Laser Deposited on Quartz Glass	104
Figure 5.20	: The J-V Graph for $\text{Si}_{0.9}\text{Ge}_{0.1}$ Effect on (a) White Light and (b) Red Light Laser Deposited on Quartz Glass	105
Figure 5.21	: The Dark and Light Illumination J-V Graph for (a) $\text{Si}_{0.8}\text{Ge}_{0.2}$ and (b) $\text{Si}_{0.9}\text{Ge}_{0.1}$ Deposited onto ITO Substrate	109

LIST OF SYMBOLS

a	- Alpha
A	- Ampere
Å	- Angstrom
β	- Beta
cm	- Centimetre
A/W	- Current per watt
°	- Degree
°C	- Degree Celsius
D	- Ens
ε	- epsilon
fA	- Farthingales
fA/cm²	- Farthingales per square centimetre
K	- Kelvin
λ	- Lambda
μm	- Micrometre
mA/cm	- Milliampere per centimetre
mW	- Milliwatt
mW/cm²	- Milliwatt per square centimetre
nm	- Nanometre
In	- Natural logarithm
Ω	- Ohm
%	- Percentage
Rad	- Radian
s	- Second
Scm⁻¹	- Siemens per centimetre
σ	- Sigma
Cm²	- Centimetre squares
Cm² V⁻¹s⁻¹	- Centimetre squares per volt second
θ	- Theta
2θ	- Two thetas

Torr	- Torricelli
V	- Volt
W	- Watt
Wt.%	- Weight percent
Ωm	- Ohm metres



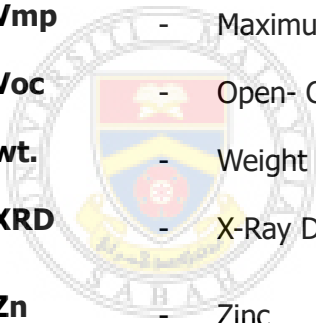
UMS
UNIVERSITI MALAYSIA SABAH

LIST OF ABBREVIATIONS

AFM	- Atomic Force Microscopy
Ag	- Silver
Al	- Aluminium
Ar	- Argon
ASCII	- American Standard Code for Information Interchange
CB	- Conductive Band
CdTe	- Cadmium Telluride
CdZnS	- Cadmium Zinc Sulphide
CPC-PV	- Compound Parabolic Concentrators- Photovoltaic
CPCs	- Compound Parabolic Concentrators Solar
DC	- Direct Current
EBIC	- Electron Beam Induced Current
E_g	- Optical Bandgap
EQE	- External Quantum Efficiency
eV	- Electron Volt
FDTD	- Finite-Difference-Time-Domain
FF	- Fill Factor
Ge	- Germanium
GO	- Graphene Oxide
GPVDM	- General Purpose Solar Cell Simulator
HTL	- Hole Transfer Layer
HTM	- Hole Transfer Material
Hz	- Hertz
IR	- Infrared

IT	- Information Technology
ITO	- Indium Tin Oxide
Jsc	- Short-Circuit Current
J-V	- Current Density - Voltage
LBIC	- Light Beam Induced Current
LiF	- Lithium Floride
mcSi	- Multi-Crystalline Silicon
MoS₂-QD	- Molybdenum Disulfide – Quantum Dots
NA	- Acceptor Density
ND	- Donor Density
NIR	- Near-Infrared
Pb	- Plumbeum
PC1D	- Personal Computer One Dimension
PCE	- Power Conversion Efficiency
PEDOT:	- Poly (3,4-ethylenedioxythiophene)
PSS	- polystyrene sulfonate
PTAA	- Poly (Triarylamine)
QE	- Quantum Efficiency
RF	- Radio Frequency
RMS	- Root Mean Square
rpm	- Revolution per Minute
R_s	- Series Resistance
R_{sh}	- Shunt-Recombination Resistance
SCAPS	- Solar Cell Capacitor Simulator
sccm	- Standard Cubic Centimetre per Minute
SC	- Solar cell

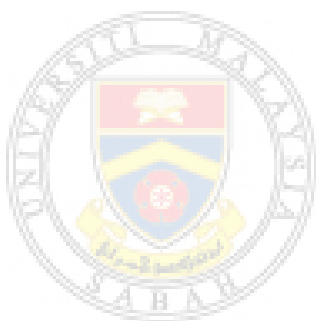
SEM EDX	- Scanning Electron Microscopy with Energy Dispersive X-Ray Spectroscopy
Si	- Silicon
SiGe	- Silicon Germanium
SILVACO	
-TCAD	- Silvaco Technology Computer Aided Design
Sn	- Tin
TCAD	- Technology Computer Aided Design
UV	- Ultra-Violet
UV-Vis	- Ultra-Violet Visible
UV-Vis-	
NIR	- Ultra Violet-Visible-Near Infrared
VB	- Valence Band
V_{mp}	- Maximum Peak Voltage
V_{oc}	- Open- Circuit Voltage
wt.	- Weight
XRD	- X-Ray Diffraction
Zn	- Zinc



UMS
UNIVERSITI MALAYSIA SABAH

LIST OF APPENDICES

	Page
Appendix A : List of Publications	132



UMS
UNIVERSITI MALAYSIA SABAH

CHAPTER 1

INTRODUCTION

1.1 Research Background

The physical properties of hybrid inorganic-organic materials have been recognised for their impressive physical properties and ability to be used as a layer in photo devices. Photo device is one of the most well-known renewable energy sources, even though it is also one of the most expensive and inefficient due to the high manufacturing cost and technologies to make solar cells as photo device. A hybrid semiconductor device offers excellent barrier and rectifying properties (Gullu, Kilicoglu, & Turut, 2010; Concilio et al., 2014; El-Shabaan & Gaml, 2022). Photo devices should not be as expensive if specific low-cost materials are utilised, as this will strengthen the photodiode business and make it more accessible to the public. It has been over a decade since photo devices were used in the country. Photo devices will reduce electric bills, and it is beneficial for the environment. Hybrid semiconductor devices reduce energy consumption, which results in lower electricity bills. By using low-cost materials, the cost of photo devices can be reduced, making them more accessible. Hybrid semiconductor devices are more efficient and can use less energy, resulting in lower electricity bills. It helps to reduce environmental impact. Additionally, this technology can be used to produce clean energy, which reduces carbon emissions and is more sustainable.

The first photo device was invented in the mid-19th century in 1856 (Popoola, 2015; Groeneveld et al., 2022). They developed the first silicon (Si) photo device with low percentage efficiency, which has resulted in a wide range of photo device bulk materials. In time, photo devices have developed, and many researchers have attempted to increase the performance of photo devices. Si cells have become a hot